A Coarse-Grained MARTINI Model of Polyethylene Glycol and of Polyoxyethylene Alkyl Ether Surfactants

ARTICLE *in* THE JOURNAL OF PHYSICAL CHEMISTRY B · NOVEMBER 2012

Impact Factor: 3.3 · DOI: 10.1021/jp3095165 · Source: PubMed

A Coarse-grained MARTINI Model of Polyethylene Glycol and of Polyoxyethylene Alkyl Ether Surfactants

G. Rossi[1,2,3,*], P. Fuchs[1,2,3], J. Barnoud[1,2,3] and L. Monticelli[1,2,3,*]

[1] INSERM, UMR-S665, Paris, F-75015, France
[2] Université Paris Diderot, Sorbonne Paris Cité, UMR-S665, Paris, F-75013, France
[3] INTS, Paris, France
*giulia.rossi@gmail.com and luca.monticelli@inserm.fr

Keywords

Self-Assembly; Membrane; Polymer; Molecular Dynamics; non-ionic surfactant

Abstract

Non-ionic surfactants are used for the isolation and purification of membrane proteins, as well as for the study of fundamental aspects of protein diffusion in membranes. Here we present a new coarse-grained model of polyethylene glycol (PEG) and of the family of polyoxyethylene alkyl ether (C_iE_j) surfactants. The model is compatible with the MARTINI coarse-grained force-field for lipids and proteins. We validate the model by comparing Molecular Dynamics simulations with experimental data. In particular, we show that the model reproduces the phase behavior of water-surfactant mixtures as a function of water concentration. We also simulate the self-assembly of two ternary mixtures that have been used for the experimental measure of protein diffusion coefficients. The first includes a co-surfactant that affects the curvature of the surfactant bilayers; the second is a mixture of C_iE_j surfactants, alkanes and water. In both cases, the results of self-assembly simulations are in agreement with experimental observations and pave the way to the use of the surfactant model in combination with MARTINI peptides and proteins.

Introduction

Non-ionic surfactants find application in many biochemical techniques for membrane and membrane protein studies[1-3]. By solubilizing the membrane, they can be used for the isolation and purification of membrane proteins or other membrane constituents. Among non-ionic surfactants, poly(oxyethylene) alkyl ethers, usually abbreviated by C_iE_j (CH_3-$(CH_2)_i$-$(O$-CH_2-$CH_2)_j$-OH), are of special importance. C_iE_j surfactants are easy to synthesize, and their properties can be tuned at will by controlling the length of the hydrophobic and hydrophilic segments of the molecule. Like other surfactants, C_iE_j can be used to purify and crystallize membrane proteins[4]. For example, $C_{12}E_8$ has been used for the 2D crystallization of Band 3 and Ca-ATPase proteins[5,6], while C_8E_4 has allowed to get a low resolution structure of bovine rhodopsin[7].

C_iE_j surfactants in water exhibit a rich phase behavior[3], which has been thoroughly characterized by experiments[8-13]. For these reasons, C_iE_j surfactants are considered as reference detergents, suitable for the study of fundamental aspects of surfactant-surfactant[14], lipid-surfactant[1] and protein-surfactant interactions[2]. They have been considered model systems for the study of membrane mechanics, as well: Kurtisovski *et al.*[15] investigated the molecular origin of membrane rigidity by x-ray scattering experiments on C_iE_j model bilayers.

C_iE_j surfactants have also been used as model bilayer-forming detergents for the study of peptide and protein diffusion and aggregation in membranes[16-19]. In these studies, the water-C_iE_j mixture was enriched by a third component, namely an alkane or a co-surfactant. The addition of alkanes[17] offers the interesting possibility to tune the thickness of the surfactant bilayers at will: alkanes permeate into the hydrophobic core of surfactant membranes and swell them. In this way, it is possible to have direct control on the hydrophobic mismatch between the diffusing protein and the surfactant membrane. Urbach and co-workers used these three-layer systems (surfactant-alkane-surfactant) to measure diffusion coefficients of peptides and proteins as a function of hydrophobic mismatch[17]. Protein diffusion measurements have been performed on a sponge phase of $C_{12}E_4$, as well[16]. In these experiments, sponge phases are obtained by combining C_iE_j surfactants with a co-surfactant, β-octylglucopyranoside (β-OG), that possesses positive spontaneous curvature and promotes the disruption of the regular lamellar phase in favor of the sponge phase. These sponge phases were used to measure the diffusion coefficient as a function of the protein size. The results, for small proteins, were in stark contrast with the well-known Saffman-Delbrück model. Applications of C_iE_j surfactants to the study of protein diffusion are of great interest for the biophysics community.

Both membrane solubilization and protein dynamics in membranes take place on time scales of at least tens of microseconds. From a modeling perspective, they are thus difficult to access by all-atom Molecular Dynamics (MD) simulations, calling for the adoption of coarse-grained approaches.

To the best of our knowledge, two coarse-grained (CG) models of C_iE_j surfactant have been proposed in the literature. Shinoda *et al.*[20-22] developed a coarse-grained model of C_iE_j surfactants, designed to reproduce density and structural properties as calculated by all-atom simulations, and thermodynamic properties (surface tension, transfer and hydration free energies) as measured experimentally. The model reproduces well the phase behavior of the surfactant. In 2009, Lee et al.[23] presented a MARTINI[24] model of polyethylene glycol (PEG), very recently combined with MARTINI alkanes into a CG model of C_iE_j surfactants[25,26]. The model has not been tested against the experimental phase behavior of the surfactant. Its angle and dihedral interactions are such that the model is stable when MD simulations are run with a time-step shorter than or equal to 8 fs, significantly shorter than

the usual 20-25 fs normally used in CG-MD simulations with the MARTINI force-field.

Here we present the development and validation of a new MARTINI coarse-grained model for PEG and for the family of nonionic poly(oxyethylene) alkyl ethers. First, we describe the parameterization of a new MARTINI model of PEG with two main features: (a) increased stability, allowing use in MD simulations with a time step of 20-25 fs (similar to all other molecules in the MARTINI force field); (b) improved consistence with the rest of the MARTINI force-field in terms of reproducing experimental partitioning data. We validate the model by verifying that the structural properties of PEG in good solvent conditions are well reproduced, as a function of the polymer molecular weight. Second, we combine the MARTINI alkanes and PEG into a C_iE_j surfactant model. The performance of the model is assessed by comparison with experimental data, and particularly with structural properties of surfactant membranes and with the phase behavior of a set of surfactant molecules in water ($C_{12}E_2$, $C_{12}E_4$, $C_{12}E_6$), assessed by means of self-assembly simulations. Third, we demonstrate the usefulness of the model for studies of protein diffusion in surfactant membranes. We simulate the self-assembly of a surfactant/water/alkane mixture and verify that the alkanes penetrate the membrane and make it thicker, in agreement with experimental data. Such systems can be used to study protein diffusion as a function of hydrophobic mismatch[17]. Finally, we describe the development of a MARTINI model for the β-OG surfactant, and we characterize its influence on the stability of the lamellar phase of C_iE_j surfactants.

The paper is structured as follows. In Section Model and Methods, the development of the PEG and C_iE_j models is described. In the Results section, we present the structural characterization of C_iE_j lamellar phase, and the outcomes of our self-assembly simulations. In the Discussion section, we discuss pros and cons of the model, in light of the comparison with experimental data and with previously available CG models of C_iE_j surfactants.

Model and methods

All simulations, both atomistic and coarse-grained, were performed with the Gromacs 4.5[27] molecular dynamics package.

Simulation protocols

Atomistic simulations. United-atom simulations of PEG and $C_{12}E_4$ in water relied on the latest GROMOS parameterization of ethers[28,29] (coined $53A6_{OXY+D}$) along with the SPC water model[30]. For $C_{12}E_4$, standard alkanes parameters of GROMOS96 were used[31]. Periodic boundary conditions were applied in all directions. The time step was set to 2 fs. The simulations were carried out at constant temperature of 300 K by means of the stochastic velocity rescale thermostat by Bussi *et al.*[32] (0.1 ps relaxation time, with

surfactant and water coupled separately), and constant pressure of 1 bar, by means of the Parrinello-Rahman[33] barostat (with a 4 ps relaxation time and a compressibility of 4.5×10^{-5} bar^{-1}, *z* coupled independently of *x* and *y* for the simulation of bilayer structures). Electrostatic interactions were handled using a twin-range scheme, with short- and long-range cutoff distances set to 0.8 and 1.4 nm, respectively. The neighbor-list was updated every 5 steps. A reaction-field correction was applied to take into account long-range electrostatics using a dielectric constant of espilon=61. More details about the all-atom simulation settings can be found in Fuchs *et al.*,[29].

CG simulations. In our standard *NpT* set-up for CG simulations we used the stochastic velocity rescale thermostat by Parrinello *et al.*[32] and a Parrinello-Rahman[33] barostat. Isotropic, semi-isotropic and anisotropic pressure coupling were applied, depending on the simulation (details are specified in the Results section). The pressure was set to 1 bar, temperature to 300 K. All CG simulations were run with a time step of 20 fs. Periodic boundary conditions were applied in all directions. The neighbor list for all non-bonded interactions was updated every 10 steps. The time scales indicated throughout the paper correspond to the formal simulated CG time, with no rescaling based on the comparison with atomistic dynamics. We recall that MARTINI is known to accelerate the dynamics of water by approximately a factor of 4[24].

Thermodynamic integration (TI). Free energies of transfer between octanol and water, at CG level, were calculated as the difference between the free energy of solvation, in water ($\Delta G_{solv\ w}$) and octanol ($\Delta G_{solv\ o}$):

$$\Delta G_{ow} = \Delta G_{solv\ w} - \Delta G_{solv\ o} \quad (1)$$

Free energies of solvations were calculated using the thermodynamic integration technique[34]. A single target molecule was inserted in a box of solvent (325 octanol molecules or 500 water molecules), then its interactions with the solvent were coupled to a parameter, λ, so that for λ=0 all the interactions were present, and for λ=1 the molecule did not interact with the solvent. In each solvent, we performed 30 runs, each one corresponding to a different value of λ and of the duration of 1 microsecond. λ values were unequally spaced to better capture the changes of slope of $\langle \partial H(\lambda)/\partial\lambda \rangle$, *H* being the Hamiltonian of the system. The value of the free energy of solvation was then obtained by integration:

$$\Delta G_{solv} = -\int_0^1 \langle \frac{\partial H(\lambda)}{\partial \lambda} \rangle_\lambda \, d\lambda \quad (2)$$

All TI simulations were performed in the *NpT* ensemble, at *T* = 298 K and atmospheric pressure conditions. A soft-core potential[35] was used for the non-bonded interactions to avoid the singularity in the potential when the interactions are turned off and molecules can overlap. Following the symbol convention of the Gromacs manual[27,36], soft-core parameters were assigned

as follows. The non-dimensional soft-core parameter α, that controls the height of the potential around r = 0, was set to 1.3. The soft-core power was *p* set to 1 and the range of the interaction (soft-core σ) was set to 0.47 nm.

New MARTINI model for PEG

Bonded interactions. To describe bonded interactions, we used harmonic (bonds), cosine-harmonic (angles) and Ryckaert-Bellemans (RB) functions (dihedrals). The parameters of the bonded interactions were tuned so as to reproduce the distributions of bonds and angles obtained from all-atom simulations, in the same fashion as for other MARTINI polymers (polystyrene [30], polyesters [31], PEG [19]).

We simulated, at atomistic level, a 27-mer PEG chain in water, a good solvent for PEG. Then, we tracked the trajectories of the center of mass of each PEG monomer, excluding the free terminal groups, and derived the distributions of the CG bonded interactions. We refined our CG parameterization using a trial-and-error procedure to achieve the best agreement between the CG distributions and the target atomistic distributions. The final parameters are reported in Table 1.

Table 1 Parameters of the bonded interactions of the PEG MARTINI model. Bonds and angles are described by harmonic functions, $V_b=(1/2)\times k_b(b-b^0)^2$ and $V_\theta=(1/2)\times k_\theta(\cos(\theta)-\cos(\theta^0))^2$, respectively. b^0 is the equilibrium value for PEG bonds, k_b is the harmonic force constant. θ^0 is the equilibrium angle, k_θ is the force constant. RB coefficients are listed from the smallest to the largest power of the series of cosines.

b^0 [nm]	k_b [kJ mol^{-1} nm^{-2}]	θ^0 [deg]	k_θ [kJ mol^{-1}]	RB parameters [kJ mol^{-1}]
0.322	7000	122	400	-2.7324; 4.3732; -0.1130; -3.6384; 0.9027; 1.1460

With respect to previous PEG parameterizations[23,37], our equilibrium values for bonds and angles are kept slightly smaller than their atomistic counterparts. This prevents instabilities due to large dihedral angle variations that might occur when the angle approaches 180°. With our set-up, stable CG simulations can be run with a time step of 20 fs.

Non-bonded interactions. MARTINI CG beads were originally parameterized[24] to reproduce the free energy of transfer between water and oil of a set of 18 different chemical building blocks. Whenever attempting the parameterization of a new molecule with the MARTINI force-field, it is good practice to verify that the chosen MARTINI beads do indeed satisfy a key requirement: they should have the same free energy of transfer between water and oil as the chemical building block they represent.
With this in mind, we proceeded to the parameterization of the PEG model. PEG monomers are C-O-C units, leading to the natural choice of a 3-to-1 mapping. MARTINI beads with a Lennard-Jones σ parameter of 0.47 nm

typically represent a 4-to-1 mapping, while smaller beads with σ=0.43 nm have been used often[23,26,37,38] to represent 2-to-1 and 3-to-1 mappings. Here, we will adopt small beads with σ=0.43 nm.

Dimethyl ether and 1,2-dimethoxyethane (DME) are the monomer and dimer units constituting CG PEG chains. Dimethyl ether partitions between octanol and water with a $\log P_{ow}$= 0.1, corresponding to a Gibbs free energy of transfer from octanol to water ΔG_{ow}=0.58 kJ/mol[24]. This value suggests that dimethyl ether might be well represented by either a MARTINI type P (ΔG_{ow} equals -1 kJ/mol for P_1 and P_2 types), or by a type N (ΔG_{ow} equals +3 kJ/mol for N_{da}, N_a, N_d and N_0). We expect that the ΔG_{ow} differences between different MARTINI beads will be enhanced when considering the partitioning behavior of their dimers, trimers, etc. We thus adopt as target for our parameterization the experimental $\log P_{ow}$ of DME, corresponding to a dimer at CG level. Table 2 reports the target experimental value of ΔG_{ow} for DME, and the same quantity as calculated by Thermodynamic Integration for a set of MARTINI dimers, built with beads belonging to the P or N class.

Table 2 Free energy of transfer between octanol and water of DME (experimental data, as reported by Funasaki *et al.*[39]), and of a set of MARTINI dimers. The bead type P_0 is not part of the original MARTINI release, but it is introduced hereby for the PEG model optimization

	DME	P_2-P_2	P_1-P_1	N_{da}-N_{da}	P_0-P_0
ΔG_{ow} [kJ/mol]	-1.21	-7.66 ± 0.02	-4.75 ± 0.02	+4.53±0.02	-0.08 ± 0.02

We remark that the N_{da} type is representative of the N_{da}, N_d and N_a types, as their interactions with MARTINI octanol and water are the same. While P_1 provides the best match with experiments, a disagreement of 4.75-1.21=3.54 kJ/mol between the simulated and experimental data is somehow larger than those typically achieved in MARTINI. We thus refined our PEG parameterization by introducing a new bead type, coined P_0, whose interactions are intermediate between those of P_1 and N_{da} beads. In particular, the strength of the Lennard-Jones interaction of the P_0 bead with water (P_4) is set to ε = 4.25 kJ/mol. This refinement leads to an optimal agreement between the simulated and experimental values of ΔG_{ow}, as reported in the last column of Table 2. Notice that for PEG we use the “small” version of this new bead type, SP_0, whose interactions with regular MARTINI beads are the same as for P_0, while interactions with other “small” beads use σ=0.43 nm and an interaction strength reduced to 0.75*ε (according to the standard MARTINI rules).

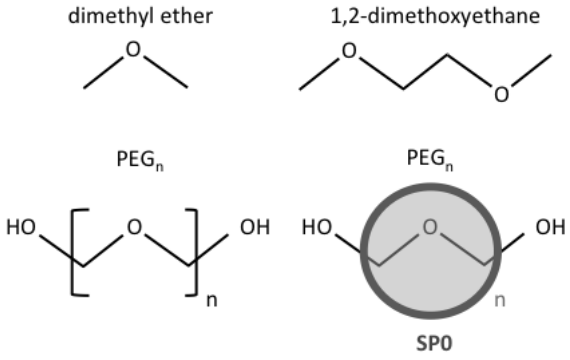

Figure 1 Top: atomistic structures of the two chemical building blocks considered as targets during the parameterization of the MARTINI PEG. Bottom: the atomistic and CG representation of PEG

PEG structure in good solvent. The radius of gyration of our model PEG was checked via simulations of single PEG molecules in water, at different chain lengths. The size of the simulation cell was set to be larger than twice the expected radius of gyration, so as to avoid interactions of the PEG molecule with its periodic image. The duration of the simulations was sufficient to reach a satisfactory equilibration of the chain conformation (1 μs, 1 μs, 3 μs, 4 μs, 5 μs and 6 μs for PEG10, 20, 50, 70, 100 and 150, respectively). Data are collected in Figure 2, where they are compared to previous experimental and computational data. There is good agreement between our CG model and the available data. A fit of our data to $f(x) = A \cdot N^{\nu}$, with the Flory exponent $\nu = 0.59$, $A =$ constant, falls within the statistical uncertainty.

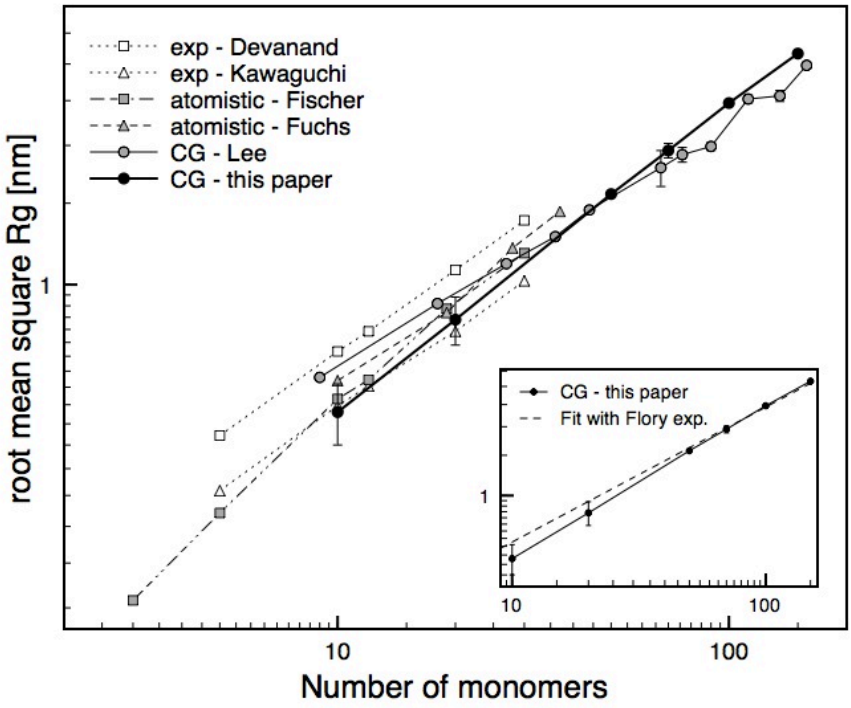

Figure 2 Radius of gyration vs. chain length. Experimental data are extrapolations to the small chain lengths from Devanand and Selser[40] and Kawaguchi *et al.*[41]. Atomistic simulation data are from Fischer *et al.*[42] and Fuchs *et al.*[29]. Coarse-grained data are from Lee *et al.*[23]

MARTINI model for C_iE_j

Bonded interactions. The alkane segment of C_iE_j molecules was parameterized as alkanes in the original MARTINI force-field. In order to get a complete topology of C_iE_j surfactants, we had to set the bonded interactions linking the alkane segment of the surfactant to the PEG segment, and the PEG segment to the terminal C-OH group. The bead representing the latter is called SP_h (see Figure 3). The equilibrium values and force constants of such interactions were assigned based on atomistic simulations of a $C_{12}E_4$ chain in water. We used a surfactant united atom model based on the latest versions of the GROMOS force field: for the polar head, we used the recent 53A6_OXY+D parameterization of polyethers[28,29] whereas for the aliphatic tails, we used standard GROMOS 53A6 alkane parameters[43].

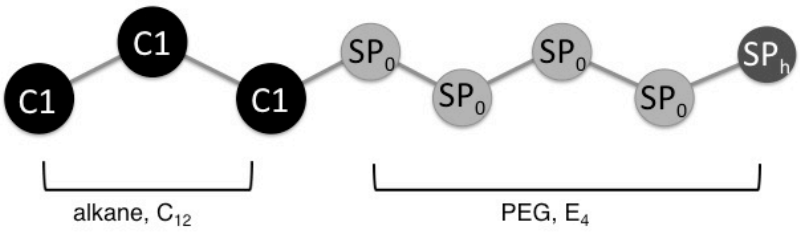

Figure 3 The CG structure of $C_{12}E_4$

Bonded interactions in the PEG segment were refined with respect to the pure PEG parameterization. Indeed, a topology with no dihedral angle and a slightly larger equilibrium angle in the PEG segment provided better performance in terms of stabilization of the lamellar phase of $C_{12}E_4$ (see the Results section). Table 3 contains all the bonded interaction parameters of our surfactant model.

Table 3 Parameters for the bonded interactions of C_iE_j molecules. C_1 is the MARTINI type for alkanes. SP_0 is the MARTINI type used in this paper for PEG. SP_h is the MARTINI type assigned to the last carboxylic group of C_iE_j molecules.

bonded interaction	equilibrium b or θ [nm] or [deg]	force constant k_b or k_θ [kJ mol^{-1} nm^{-1}] or [kJ mol^{-1}]
C_1-C_1	0.47	1250
C_1-SP_0	0.41	5000
SP_0-SP_0	0.33	7000
SP_0-SP_h	0.28	7000
C_1-C_1-C_1	180	25
C_1-C_1-SP_0	180	25
C_1-SP_0- SP_0	180	25
SP_0-SP_0-SP_0	135	200
SP_0-SP_0-SP_h	140	25

Non-bonded interactions. For the alkane segment of the surfactant molecules, we relied on the MARTINI parameterization (type C1). For the PEG segment, the type SP_0 was used, as described above.
According to our 3-to-1 mapping, where each CG bead represents a C-O-C group, one further CG bead is needed to represent the terminal C-OH group. The presence of the OH group again suggests choosing the bead type among the polar class (P) of MARTINI. The SP_0 bead type used for the rest of the PEG segment, though, does not allow for the stabilization of the lamellar phase of $C_{12}E_4$. This is an important test for the force-field, as the phase diagram of $C_{12}E_4$-water mixtures is characterized by a wide lamellar region at room temperature, as shown in the Results section. In simulations using the terminal SP_0 bead, big pores open in the lamellar structure, which is disrupted on a time scale of hundreds of nanoseconds.
We thus proceeded to a rather systematic variation of the strength of the non-bonded interactions of the terminal bead. We eventually changed only the self-interaction, which was made more attractive than the regular SP_0-SP_0 interaction (ε = 3.75 kJ/mol instead of 3.375 kJ/mol). All other interactions were set to the same levels as the SP_0 interactions.

Results

Validation of the C_iE_j model

We validated the C_iE_j MARTINI model by verifying to what extent it is able to reproduce the phase diagram of three widely used surfactant molecules, $C_{12}E_2$, $C_{12}E_4$ and $C_{12}E_6$. They all have a rich phase behavior when mixed with

water. Above the critical micelle concentration (CMC), self-assembly gives rise to micellar, hexagonal, cubic and lamellar phases, depending on the surfactant concentration and temperature.

Figure 4 shows the main features of the phase diagrams of $C_{12}E_2$, as reported by Funari and Rapp[9] and of $C_{12}E_4$ and $C_{12}E_6$, as reported by Mitchell[8]. Phase W contains surfactant molecules dissolved in water. The L_2 phase, which is liquid surfactant containing dissolved water, is characterized by a very broad scattering peak, reflecting a wide range of distances[9]. As W and L_2 concern areas of the phase diagram where the temperature is much higher than the physiological temperature, or the surfactant concentration is either extremely high or extremely low, we did not use them as targets for the validation of the CG model. We did not aim at reproducing cubic phases either; the direct (V_1) and the inverse cubic phase (V_2) occupy a narrow region of the phase diagram, and are therefore difficult to reproduce with any simulation model. Instead, we focused on the lamellar (L_α), hexagonal (H_1) and micellar (L_1) regions of the phase diagrams.

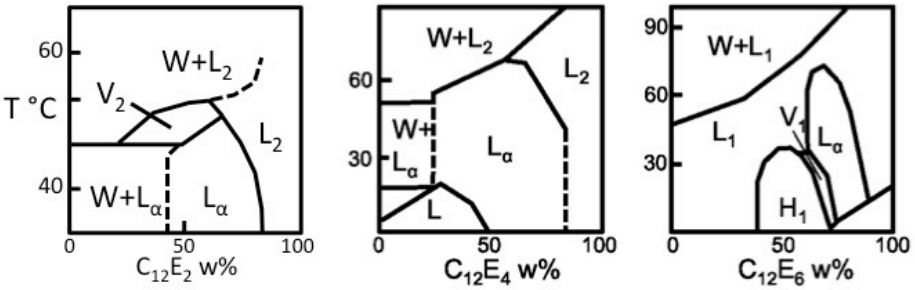

Figure 4 From left to right: water-surfactant phase diagrams for $C_{12}E_2$, $C_{12}E_4$ and $C_{12}E_6$. The x axis reports the weight percentage of surfactant in the mixture. Phase diagrams have been re-drawn and simplified compared to the original figures reported in[9] and[8].

Lamellar phases. At 300 K, lamellar configurations occupy most of the phase diagram of $C_{12}E_4$, from 20% to 80% of surfactant content (w%, percentage of surfactant weight). For $C_{12}E_2$ and $C_{12}E_6$, lamellae are observed in the 40-80 w% and 70-85 w% range, respectively. We thus checked the stability of the lamellar configuration of $C_{12}E_2$ (70 w%), $C_{12}E_4$ (30, 50 and 70 w%) and $C_{12}E_6$ (80 w%). We performed long runs of pre-formed lamellae containing 392 surfactant molecules. Simulations were carried out with semi-isotropic pressure coupling, so as to decouple the action of the barostat in the direction perpendicular and parallel to the membrane. In all cases, the lamellae were stable along the whole 5-microsecond duration of the run.

Table 4 reports the structural data of the simulated lamellar configurations, and a comparison with experiments. The area per surfactant is defined as the ratio between the average *x* and *y* edges of the simulation box, divided by the number of surfactant molecules per leaflet. The thickness of the hydrophobic core of the lamella, h_t, is here defined as the distance between the crossing

points of the PEG and alkane densities, along the membrane normal, as shown in Figure 5 for the case of $C_{12}E_2$, 70 w%.

Self-assembly of lamellar, hexagonal and micellar phases. To further confirm the reliability of the model at reproducing the phase diagrams shown in Figure 4, we performed a series of self-assembly simulations at the temperature of 300 K. These runs were started from random distributions of the molecules, and lasted between 3 and 5 microseconds. Self-assembly simulations are listed in Table 5, while some of the resulting structures are shown in Figure 6. The lamellar phase of $C_{12}E_2$ confirmed to be very stable, with 5 successes out of 5 self-assembly simulations (Figure 6, a). The lamellar phase of $C_{12}E_4$ at the relatively high hydration of 50%, proved to be a more severe test. None of the self-assembly runs formed a perfect lamellar structure, but 3 out of 6 showed the formation of lamellar structures with pore defects (Figure 6, b).

Table 4 Area per surfactant molecule and thickness of the hydrophobic core in lamellar configurations of $C_{12}E_2$, $C_{12}E_4$ and $C_{12}E_6$. The error on the area per surfactant, as derived from the area fluctuations, is of the order of 10^{-3} nm^2 or smaller. The error on the hydrophobic thickness, h_t is of the order of 10^{-2} nm, estimated by measuring h_t along two halves of the simulation and averaging the results. *The experimental data refer to surfactant weight percentage intermediate between 50% and 70%. **Different surfactant weight percentages were tested, assuming no dependence of the area per molecule on the water concentration

	$C_{12}E_2$ 70%	$C_{12}E_4$ 30%	$C_{12}E_4$ 50%	$C_{12}E_6$ 80%
area per surfactant molecule [nm^2]				
Experimental	0.30[9] 0.33[15]**		0.42[44] 0.41[15]**	>0.43[15] 0.48[44]
CG simulation	0.314	0.362	0.371	0.374
hydrophobic thickness [nm]				
Experimental	2.26[9] 2.16[15]		1.5[44]* 1.72[15]**	1.4[44]
CG simulation	2.16		1.86	1.81

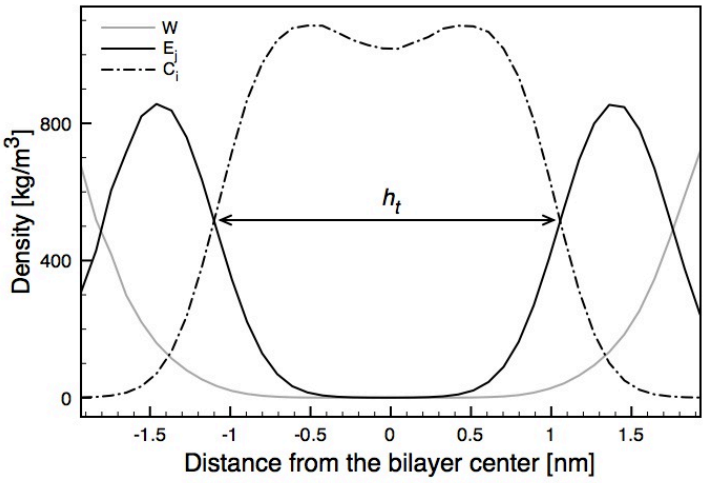

Figure 5 Density profiles of water (W) and of the PEG (E_i) and alkane (C_i) segments of a water-$C_{12}E_2$ lamellar phase.

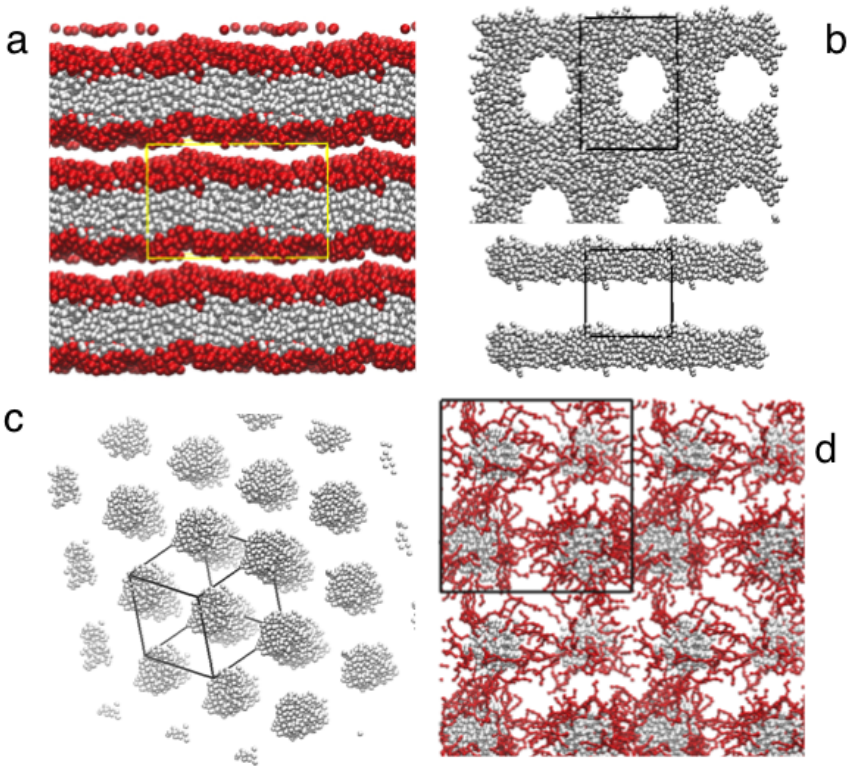

Figure 6 Structures formed via self-assembly simulations. The periodic simulation box is shown in yellow (a) or black (b, c and d), water is not shown. a) Lamellar phase of $C_{12}E_2$ at 70 w% water content. Alkane and PEG beads are grey and red, respectively. b) Lamellar phase of $C_{12}E_4$, with pores, at 50 w%. Only alkane beads are shown. Both a top and a lateral view are shown. c) Hexagonal phase of $C_{12}E_6$, at 50 w%. Only alkane beads forming the core of cylindrical micelles are shown. d) Micellar phase of $C_{12}E_6$ at 20 w%. Alkane beads are white, PEG segments are red.

The self-assembly simulations of $C_{12}E_6$-water mixtures were successful at all the hydration levels considered. At very high hydration, the model predicts the formation of a micellar phase (Figure 6, d). The model correctly describes the self-assembly and stabilization of the hexagonal phase, as well (Figure 6, c). At 50% hydration, the self-assembly runs that did not converge to an ideal hexagonal phase yielded tubular periodic micelles. These tubular micelles share the same curvature as hexagonal phases and appear to represent a metastable state, which can probably evolve into hexagonal symmetry on a longer time scale.

In order to better characterize the micellar phase of $C_{12}E_6$ in terms of micellar size and distributions, we performed three long runs (10 microseconds) of a larger system containing 1728 surfactant molecules at 20% weight concentration. As shown in Figure 7, the average size of the micelles after 10 microseconds set to N=60 surfactant molecules, while the size distribution remained wide on this time scales ($40 < N < 160$). In particular, in one of the simulations a fusion event between two large micelles took place after 7.5 microseconds. Snapshots from the fusion event are shown in Figure 8. Such a behavior suggests that the convergence of the average micelle size might not have been reached yet.

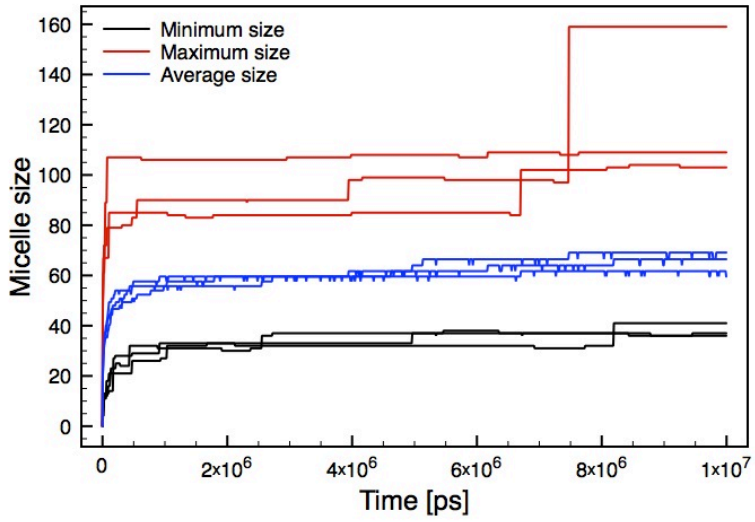

Figure 7 Aggregation data from three large self-assembly simulations of $C_{12}E_6$ at 20% weight concentration. The size (number of surfactant molecules) of the largest micelle is shown in red, that of the smallest in black. The average micelle size is shown in blue.

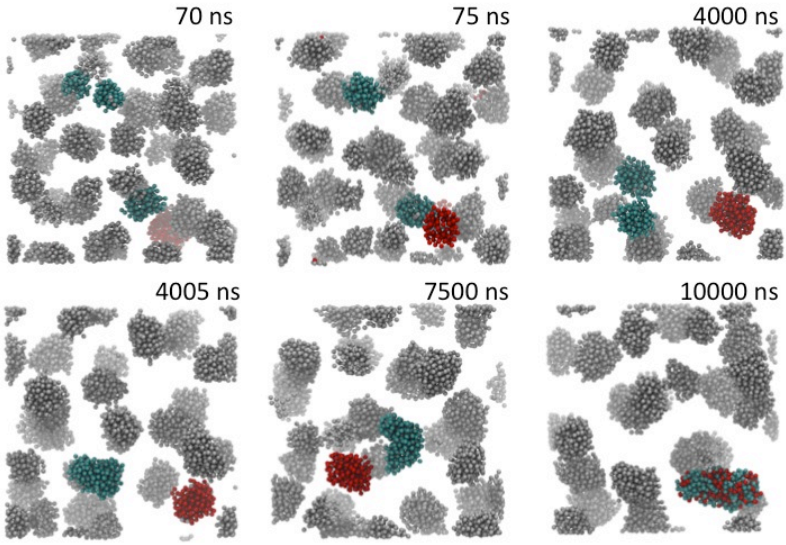

Figure 8 Snapshots from a 10 microsecond run in the micellar phase of $C_{12}E_6$. Only alkane beads are shown. Fusion events between the red and cyan micelles are shown. At first (top, left) one red micelle and three cyan micelles are present in the box. Then, the cyan micelles fuse into a single larger one. After 7.5 microseconds (bottom, center) the red and the cyan micelles approach each other and fuse into a rod-shaped micelle containing 160 surfactant molecules.

Self-assembly of $C_{12}E_2$ in presence of dodecane. The hydrophobic mismatch between the thickness of lipid membranes and the trans-membrane domain of peptides and proteins is known to affect both the orientation of the insertion and the lipid ordering[17]. Mixtures of alkanes and C_iE_j surfactants offer the possibility to tune at will the thickness in synthetic membranes. Alkanes diffuse into the hydrophobic region of the bilayer, and by controlling the amount of alkanes in the system it is possible to control the thickness of the resulting lamellar phase.

We have thus simulated the self assembly of a 1:1:1 dodecane:$C_{12}E_2$:water mixture. Starting as usual from a random distribution of the three components, the system self-assembles into a lamellar structure, with all dodecane molecules comprised between the polar segments of the surfactant.

Table 5 Self-assembly simulations. N_{surf} is the number of surfactant molecules in the simulation box. Either a semi-isotropic (semi-iso, *z* coupled independently of *x* and *y*) or isotropic (iso) pressure coupling was applied. For $C_{12}E_4$ at 50 w%, the self-assembled lamellae contained pores.

	w%	N_{surf}	barostat	run time [μs]	expected structure	success
$C_{12}E_2$	70	216	semi-iso	3	lamellar	5/5
$C_{12}E_4$	50	216	semi-iso/iso	5	lamellar	3/6
$C_{12}E_6$	80	216	semi-iso	3	lamellar	3/4
$C_{12}E_6$	50	216	semi-iso/iso	≥ 3	hexagonal	2/5
$C_{12}E_6$	20	216	iso	≥ 3	micellar	3/3
$C_{12}E_6$	20	1728	iso	10	micellar	3/3
$C_{12}E_2$-β-OG	70	216	semi-iso	3	sponge	2/5

Self-assembly of $C_{12}E_2$ in presence of β-OG. In order to verify the influence of the β-OG co-surfactant on the stabilization of the sponge phase for C_iE_j surfactants, we developed a MARTINI model of β-OG and performed some self-assembly simulations of β-OG-$C_{12}E_2$-water mixtures. As shown in Figure 9, we adapted the MARTINI model of disaccharides[45] replacing the second sugar ring with the alkane tail of β-OG. The topology does not include any dihedral angle, while all other bonded interactions are as reported in Ref.[45] and[24].

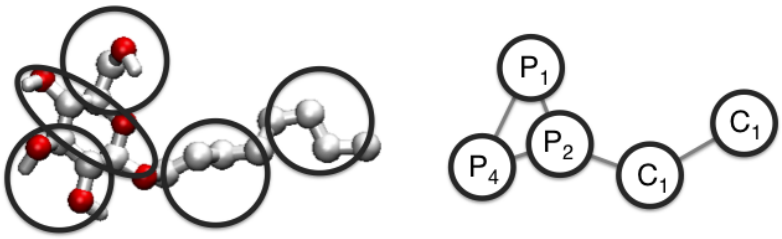

Figure 9 Left: atomistic structure of β-OG. Grey circles include the atoms which center of mass has been mapped onto the CG beads. Right: CG description of β-OG. P_1, P_2, P_4 and C_1 are the names of the MARTINI types used in the model.

We performed a set of five self-assembly simulations, on a 1:3:3 β-OG-$C_{12}E_2$-water mixture. The results are reported in Table 5. $C_{12}E_2$ had showed a strong tendency to form lamellae at 70 w%, with 5 out of 5 self-assembly simulations leading to the formation of a perfect lamellar structure (see Table 5). The presence of 10% β-OG, though, affects this behavior significantly. In 2 cases out of 5, β-OG aggregates and "pinches" the lamellae, confining the water phase to flat tubular domains (see the right panel of Figure 10). In the remaining runs, β-OG does not aggregate and the lamellar structure is not perturbed (see the left panel of Figure 10).

Discussion

In this paper we presented the development of coarse-grained models of the C_iE_j family of non-ionic surfactants. C_iE_j surfactants consist of a hydrophobic alkane segment linked to a polar polyethyleneoxide chain. Our model relies on the MARTINI parameterization of alkanes and on a newly developed MARTINI model for PEG. Non-bonded interaction parameters of the new PEG beads are assigned based on the free energy of partitioning of a PEG dimer, namely 1,2-dimethoxyethane, between water and octanol. This procedure is consistent with the parameterization of the MARTINI force-field, and guarantees compatibility with the large set of lipids[24], proteins[46], sugars[45], polymers[38,47,48] and carbon nanoparticles[49,50] for which a MARTINI model is available.

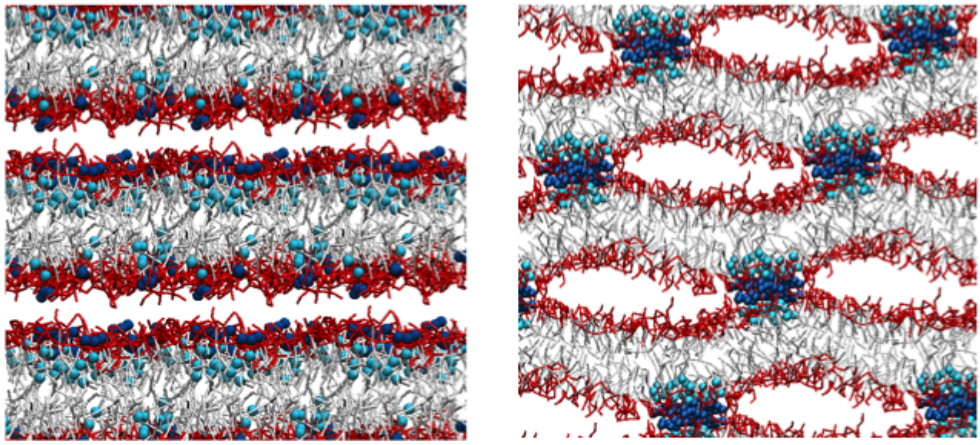

Figure 10 Output configurations of the self-assembly runs of β-OG-$C_{12}E_2$-water mixtures. PEG and alkane segments of $C_{12}E_2$ are shown by grey and red sticks, respectively. The beads of the polar heads of β-OG are shown in dark blue, the alkane tails in cyan. Water is not shown. On the left, β-OG is not aggregated and does not affect the lamellar structure of the surfactant. On the right, β-OG aggregates and induces pinching of the lamellae.

In the literature, other MARTINI parameterizations of PEG can be found[23,37]. It is worth analyzing here in more detail the differences between these previous models and the present one. In the first paper by Lee *et al.*[23], the non-bonded parameters for PEG beads were based on the experimental density of low molecular weight PEG and the radius of gyration of PEG oligomers in water, as obtained from atomistic simulations. The bead chosen to represent PEG monomers was a combination of SN_{da} (for self-interactions) and SN_a (for interactions with the solvent) MARTINI types. The free energy of transfer between water and octanol for PEG dimers represented by two SN_a beads is +4.53 kJ/mol, to be compared with -1.21 kJ/mol obtained experimentally (see Table 2); it differs by 5.7 kJ/mol from the target experimental value, and it has the wrong sign (partitioning in octanol is preferred over water). This model,

originally developed by Lee *et al*., was recently refined in a study of PEGylated lipids[37]. The authors modified the non-bonded parameters for the SN_a particle type in an *ad hoc* fashion, by reducing specifically the strength of the interaction with the C_1 alkane beads. The refinement was motivated by the failure of the first model to reproduce the thickness of the PEG layer on PEGylated lipids, and was not based on the partitioning behavior of PEG beads. This second model by Lee[37] could qualitatively reproduce the mushroom-like behavior of PEG chains adsorbed on lipid bilayers. Incidentally, such refinement also improved the partitioning properties for DME (ΔG_{ow} = -0.9 kJ/mol). The main difference between our PEG model and the latest model by Lee et al. lies in the possibility to use a larger time step in MD simulations (20-25 fs instead of 8 fs). In all other respects, the two parameterizations are likely to give similar performance.

We completed the parameterization of C_iE_j surfactants by assigning the non-bonded interactions of the terminal polar bead, representing a C-OH group. We soon realized that the self-interactions of this terminal bead are crucial to assure the stability of the lamellar phase of C_iE_j surfactants. Such stability is indeed affected by two opposing enthalpic factors: a strong interaction with water favors the hydration of the surfactant head region; this lowers the line tension at the bilayer edge and favors the formation of pores or the disruption of the bilayer. On the contrary, a strong self-interaction of the terminal beads can counterbalance an excessive hydration of the head region and provide stability to the lamellar configuration, via an increase of the line tension at the bilayer edge. During the parameterization procedure, we calculated the line tension of several alternative models according to the protocol described in the Supplementary Material of ref.[51]. We observed that small variations of the non-bonded interactions of the terminal beads led to very significant variations of the line tension of $C_{12}E_2$ bilayers, in the 25-50 pN range; only values of about 45 pN or larger assured sufficient stability of lamellar configurations. The final parameterization, with the self-interaction of the last SP_h bead increased to 3.75 kJ/mol, yields indeed a line tension of 45 +/-3 pN.

Our model can be compared to the experimental data concerning the critical micelle concentration (CMC) for the C_iE_j family. The CMC can be related to the difference in interaction free energy by the relation[52,53]:

$$\mu_1^0 - \mu_N^0 = -RT \ln(CMC) \quad (3)$$

where μ_1^0 and μ_N^0 are the free energies of the molecule when isolated in water and when part of an N-molecule aggregate, respectively, and the CMC is expressed in mole fraction units. The CMC can be thus estimated *in silico* by calculating the free energy of transfer of a single surfactant molecule from water into a micelle (also known as free energy of desorption). We performed the calculation, by means of thermodynamic integration, for a $C_{12}E_6$ molecule. As usual, the calculation consists of two steps: (1) transfer of the surfactant molecule from the water phase to vacuum, and (2) transfer from vacuum to the micellar phase. The micelle was formed by 65 $C_{12}E_6$ molecules at 20%

weight concentration, a size consistent with the average size of $C_{12}E_6$ micelles (see below for details).

Based on the CMC value reported experimentally, namely 1.6 10^{-6} mole fractions at 298 K[54], we would expect a free energy difference between the isolated and the aggregated state of -33 kJ/mol. Our model underestimates this free energy difference, yielding -22.5 kJ/mol. A C_iE_j model based on MARTINI alkanes and on the latest release of the PEG model by Lee *et al.*[37] provides a free energy difference around -27.7 kJ/mol, better than our result but still over 5 kJ/mol below the experimental value. Nevertheless, the model by Lee suffers from the same time step limitation (8 fs) as reported for the previous PEG model[23].

We validated our model by showing how it reproduces the complex phase diagram of C_iE_j-water mixtures for three different surfactant molecules: $C_{12}E_2$, $C_{12}E_4$, $C_{12}E_6$. This is a rather severe test, as these three molecules show little difference from each other at CG level. The small number of particles at CG levels reduces the number of accessible conformations of the molecule. This might affect the phase behavior via, for example, imperfect reproduction of the spontaneous curvature of the molecule as the length of its polar segment varies.

Our simulations, either starting from pre-formed lamellar structures or from disordered mixtures of surfactant and water, were run for typical time scales of 5 microseconds, amounting to a total simulation time of about 150 microseconds. Most of the times the final configuration was reached within the first microsecond, and remained unchanged for the remaining 4 microseconds. Nevertheless, we cannot rule out the possibility that the systems got stuck in metastable configurations. This appears as an intrinsic limitation of our approach, only partially compensated by the performance of several simulations replicas (see Table 5).

The results of our self-assembly simulations are very encouraging. The lamellar phases of $C_{12}E_2$, $C_{12}E_4$ and $C_{12}E_6$ proved to be all very stable at low hydration levels, consistently with experimental observations. The comparison with experimental structural data for the lamellar phases, as reported in Table 4, is excellent for $C_{12}E_2$ in terms of both area per molecule and thickness of the lamella. When increasing the length of the hydrophilic segment, the agreement between our data and the experiments is less good. In particular, for $C_{12}E_6$ we observe a saturation of the area per lipid to a value between 0.37 and 0.38 nm^2. Experimental data collected from the same source, e.g. the SAXS measurements performed by Kurtisovski *et al.*[15], also point to a saturation of the area per lipid as the length of the hydrophilic segment increases, but the value of the area is larger, > 0.43 nm^2.

The model is able to capture complex structural changes as the water content is varied. At high surfactant concentration the lamellar configuration is stable for all the three molecules considered. At intermediate concentrations, $C_{12}E_6$

forms a hexagonal phase, well captured by our CG model. At the opposite end of the phase diagram, for the case of $C_{12}E_6$, we reported the formation of a micellar configuration. Experimental and simulation data (obtained with an implicit solvent model) suggest for this surfactant an average micelle size of N ~ 140[55]. Our long (10 μs) simulations of $C_{12}E_6$ in the micellar region of the phase diagram led to the formation of micelles with an average size of about 60 surfactant molecules, and a very wide size distribution ($40 < N < 160$). A large micelle with N=160 surfactant molecule is formed after 7 μs as a consequence of the fusion between two large micelles (see Figure 8). This micelle adopts a rod-like shape, consistently to what previously reported by Velinova *et al.*[25] at the same concentration and micelle size. The observation of micelle fusion events after 7 μs and the wide distribution of micelle sizes suggest that significantly longer simulations are necessary to predict the equilibrium distribution of micellar sizes.

Surfactants of the C_iE_j family have been used experimentally to measure protein diffusion in model membranes. In view of possible future applications of the model, we performed two sets of self-assembly simulations of ternary mixtures containing C_iE_j surfactants. The first concerns a dodecane-$C_{12}E_2$-water mixture. The addition of alkanes to C_iE_j in solution has interesting applications, as by tuning the amount of alkanes it is possible to control the thickness of the surfactant bilayer. This procedure has been used experimentally to study the diffusion of model peptides into lamellar phases of C_iE_j[17] as a function of membrane thickness. Our MARTINI models of alkanes and $C_{12}E_2$ behave as expected, with the alkanes, initially placed at random positions in the simulation box, quickly self-assembling into the hydrophobic core of the surfactant bilayer.

The second ternary mixture we looked at consisted of $C_{12}E_2$, water and a co-surfactant, β-OG. This co-surfactant is known to disrupt the lamellar phase of $C_{12}E_2$ surfactants and to favor the formation of sponge phases, used experimentally to measure diffusion coefficients of membrane proteins[16,17]. $C_{12}E_2$ proved to have a very stable lamellar phase at low hydration levels (see Table 5), and it is thus an excellent test system to verify the influence of β-OG. Self-assembly simulations of $C_{12}E_2$ in the presence of 10% β-OG yielded two alternative metastable states. In some cases, β-OG molecules remained well dispersed in the membrane throughout the simulation and the lamellar structure remained stable. In other cases, on the contrary, β-OG molecules clustered together and the lamellar structure was disrupted. This latter behavior is consistent with experimental observations[16,17] and suggests that the modification of the bilayer curvature is the result of a cooperative process, as already observed for curvature-inducing model proteins[56] and fusogenic peptides[57].

Conclusions

In the present work we have described the development and validation of a new MARTINI model for PEG and for the family of C_iE_j surfactants. To

represent PEG polymers we introduced a new bead type, coined P_0, which provides water-octanol partitioning behavior in agreement with available experimental data. The C_iE_j model performs well in reproducing the water-surfactant phase behavior, and captures the stabilization of the different phases obtained with surfactants of different hydrophilic length.
Our self-assembly simulations in water and in ternary mixtures confirm the compatibility of the model both with alkanes and with another non-ionic detergent, β-OG. Last but not least, the model is computationally as efficient as most other MARTINI models, allowing for the use of a 20-25 fs time step in MD simulations. This paves the way to the simulation of slow processes, such as peptide and protein diffusion in model membranes, taking place on time scales of tens or hundreds of microseconds.

Acknowledgments

The authors acknowledge W. Urbach and N. Taulier for insightful discussion on the experimental characterization of CiEj surfactant phases and their application to the study of membrane proteins. This work was performed using HPC resources from GENCI-CINES (Grant 2011-076353 and 2012-076353). G. Rossi acknowledges funding from the FP7 Marie Curie IEF program.

References

(1) Heerklotz, H. *Q. Rev. Biophys.* **2008**, *41*, 205-264.

(2) Rigaud, J. L.; Chami, M.; Lambert, O.; Levy, D.; Ranck, J. L. *Biochim. Biophys. Acta-Biomembr.* **2000**, *1508*, 112-128.

(3) Garavito, R. M.; Ferguson-Miller, S. *J. Biol. Chem.* **2001**, *276*, 32403-32406.

(4) Garavito, R. M.; Picot, D. *Methods* **1990**, *1*, 57-69.

(5) Lacapere, J. J.; Stokes, D. L.; Olofsson, A.; Rigaud, J. L. *Biophys. J.* **1998**, *75*, 1319-1329.

(6) Wang, D. N.; Sarabia, V. E.; Reithmeier, R. A. F.; Kuhlbrandt, W. *EMBO J.* **1994**, *13*, 3230-3235.

(7) Unger, V. M.; Schertler, G. F. X. *Biophys. J.* **1995**, *68*, 1776-1786.

(8) Mitchell, D. J.; Tiddy, G. J. T.; Waring, L.; Bostock, T.; McDonald, M. P. *Journal of the Chemical Society-Faraday Transactions I* **1983**, *79*, 975-1000.

(9) Funari, S. S.; Rapp, G. *J. Phys. Chem. B* **1997**, *101*, 732-739.

(10) Funari, S. S.; Holmes, M. C.; Tiddy, G. J. T. *J. Phys. Chem.* **1994**, *98*, 3015-3023.

(11) Fairhurst, C. E.; Holmes, M. C.; Leaver, M. S. *Langmuir* **1997**, *13*, 4964-4975.

(12) Lynch, M. L.; Kochvar, K. A.; Burns, J. L.; Laughlin, R. G. *Langmuir* **2000**, *16*, 3537-3542.

(13) Bulut, S.; Gonzalez-Perez, A.; Olsson, U. *Langmuir* **2008**, *24*, 22-25.

(14) Fernandez, P.; Willenbacher, N.; Frechen, T.; Kuhnle, A. *Colloids and Surfaces a-Physicochemical and Engineering Aspects* **2005**, *262*, 204-210.

(15) Kurtisovski, E.; Taulier, N.; Ober, R.; Waks, M.; Urbach, W. *Phys. Rev. Lett.* **2007**, *98*.

(16) Gambin, Y.; Lopez-Esparza, R.; Reffay, M.; Sierecki, E.; Gov, N. S.; Genest, M.; Hodges, R. S.; Urbach, W. *Proc. Natl. Acad. Sci. U. S. A.* **2006**, *103*, 2098-2102.

(17) Gambin, Y.; Reffay, M.; Sierecki, E.; Homble, F.; Hodges, R. S.; Gov, N. S.; Taulier, N.; Urbach, W. *J. Phys. Chem. B* **2010**, *114*, 3559-3566.

(18) Taulier, N.; Nicot, C.; Waks, M.; Hodges, R. S.; Ober, R.; Urbach, W. *Biophys. J.* **2000**, *78*, 857-865.

(19) Reffay, M.; Gambin, Y.; Benabdelhak, H.; Phan, G.; Taulier, N.; Ducruix, A.; Hodges, R. S.; Urbach, W. *Plos One* **2009**, *4*, e5035.

(20) Shinoda, W.; Devane, R.; Klein, M. L. *Mol. Simul.* **2007**, *33*, 27-36.

(21) Shinoda, W.; DeVane, R.; Klein, M. L. *Soft Matter* **2008**, *4*, 2454-2462.

(22) Klein, M. L.; Shinoda, W. *Science* **2008**, *321*, 798-800.

(23) Lee, H.; de Vries, A. H.; Marrink, S. J.; Pastor, R. W. *J. Phys. Chem. B* **2009**, *113*, 13186-13194.

(24) Marrink, S. J.; Risselada, H. J.; Yefimov, S.; Tieleman, D. P.; de Vries, A. H. *J. Phys. Chem. B* **2007**, *111*, 7812-7824.

(25) Velinova, M.; Sengupta, D.; Tadjer, A. V.; Marrink, S. J. *Langmuir* **2011**, *27*, 14071-14077.

(26) Velinova, M.; Tsoneva, Y.; Ivanova, A.; Tadjer, A. *J. Phys. Chem. B* **2012**, *116*, 4879-4888.

(27) Hess, B.; Kutzner, C.; van der Spoel, D.; Lindahl, E. *J. Chem. Theory Comput.* **2008**, *4*, 435-447.

(28) Horta, B. A. C.; Fuchs, P. F. J.; van Gunsteren, W. F.; Hunenberger, P. H. *J. Chem. Theory Comput.* **2011**, *7*, 1016-1031.

(29) Fuchs, P. F. J.; Hansen, H. S.; Hünenberger, P. H.; Horta, B. A. C. *J. Chem. Theory Comput.* **2012**.

(30) Hermans, J.; Berendsen, H. J. C.; Vangunsteren, W. F.; Postma, J. P. M. *Biopolymers* **1984**, *23*, 1513-1518.

(31) Schuler, L. D.; Daura, X.; van Gunsteren, W. F. *Journal of Computational Chemistry* **2001**, *22*, 1205-1218.

(32) Bussi, G.; Donadio, D.; Parrinello, M. *J. Chem. Phys.* **2007**, *126*.

(33) Parrinello, M.; Rahman, A. *J. Appl. Phys.* **1981**, *52*, 7182-7190.

(34) Leach, A. R. *Molecular Modelling: Principles and Applications*; Prentice Hall, 2001.

(35) Beutler, T. C.; Mark, A. E.; Vanschaik, R. C.; Gerber, P. R.; Van Gunsteren, W. F. *Chem. Phys. Lett.* **1994**, *222*, 529-539.

(36) Gromacs 4.5 manual; Vol. 2012.

(37) Lee, H.; Pastor, R. W. *J. Phys. Chem. B* **2011**, *115*, 7830-7837.

(38) Rossi, G.; Monticelli, L.; Puisto, S. R.; Vattulainen, I.; Ala-Nissila, T. *Soft Matter* **2011**, *7*, 698-708.

(39) Funasaki, N.; Hada, S.; Neya, S.; Machida, K. *The Journal of Physical Chemistry* **1984**, *88*, 5786-5790.

(40) Devanand, K.; Selser, J. C. *Macromolecules* **1991**, *24*, 5943-5947.

(41) Kawaguchi, S.; Imai, G.; Suzuki, J.; Miyahara, A.; Kitano, T. *Polymer* **1997**, *38*, 2885-2891.

(42) Fischer, J.; Paschek, D.; Geiger, A.; Sadowski, G. *J. Phys. Chem. B* **2008**, *112*, 13561-13571.

(43) Oostenbrink, C.; Villa, A.; Mark, A. E.; Van Gunsteren, W. F. *Journal of Computational Chemistry* **2004**, *25*, 1656-1676.

(44) Klose, G.; Eisenblatter, S.; Galle, J.; Islamov, A.; Dietrich, U. *Langmuir* **1995**, *11*, 2889-2892.

(45) Lopez, C. A.; Rzepiela, A. J.; de Vries, A. H.; Dijkhuizen, L.; Hunenberger, P. H.; Marrink, S. J. *J. Chem. Theory Comput.* **2009**, *5*, 3195-3210.

(46) Monticelli, L.; Kandasamy, S. K.; Periole, X.; Larson, R. G.; Tieleman, D. P.; Marrink, S. J. *J. Chem. Theory Comput.* **2008**, *4*, 819-834.

(47) Rossi, G.; Giannakopoulos, I.; Monticelli, L.; Rostedt, N. K. J.; Puisto, S. R.; Lowe, C.; Taylor, A. C.; Vattulainen, I.; Ala-Nissila, T. *Macromolecules* **2011**, *44*, 6198-6208.

(48) Milani, A.; Casalegno, M.; Castiglioni, C.; Raos, G. *Macromol. Theory Simul.* **2011**, *20*, 305-319.

(49) Monticelli, L. *J. Chem. Theory Comput.* **2012**, *8*, 1370-1378.

(50) Wong-Ekkabut, J.; Baoukina, S.; Triampo, W.; Tang, I. M.; Tieleman, D. P.; Monticelli, L. *Nat. Nanotechnol.* **2008**, *3*, 363-368.

(51) Baoukina, S.; Monticelli, L.; Risselada, H. J.; Marrink, S. J.; Tieleman, D. P. *Proc. Natl. Acad. Sci. U. S. A.* **2008**, *105*, 10803-10808.

(52) Israelachvili, J. N. *Intermolecular and Surface Forces*; Academic Press, 1992.

(53) Tieleman, D. P.; Marrink, S. J. *J. Am. Chem. Soc.* **2006**, *128*, 12462-12467.

(54) Daful, A. G.; Baulin, V. A.; Avalos, J. B.; Mackie, A. D. *J. Phys. Chem. B* **2011**, *115*, 3434-3443.

(55) Jusufi, A.; Sanders, S.; Klein, M. L.; Panagiotopoulos, A. Z. *J. Phys. Chem. B* **2011**, *115*, 990-1001.

(56) Reynwar, B. J.; Illya, G.; Harmandaris, V. A.; Muller, M. M.; Kremer, K.; Deserno, M. *Nature* **2007**, *447*, 461-464.

(57) Fuhrmans, M.; Marrink, S. J. *J. Am. Chem. Soc.* **2012**, *134*, 1543-1552.

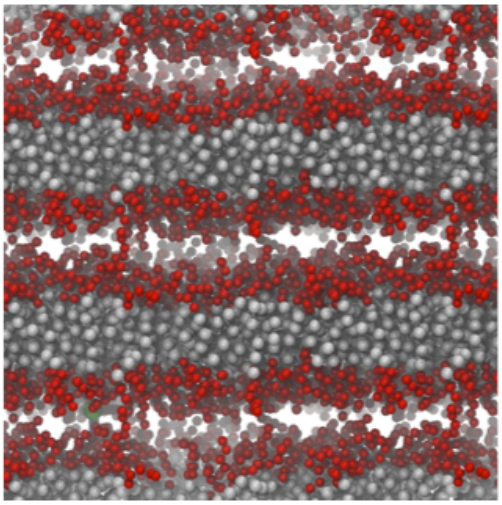

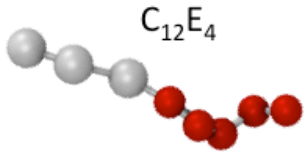

A coarse-grained MARTINI model of the non-ionic surfactants polyoxyethylene alkyl ethers. The model reproduces well the water-surfactant phase diagram of the C_iE_j molecules. A lamellar phase of $C_{12}E_4$ is shown on the left.